# α-Synuclein binds extracellular complex N-linked glycans

Melissa Birol[1], Slawomir P. Wojcik[2], Andrew D. Miranker[2] and Elizabeth Rhoades*[2]

[1]Department of Chemistry, University of Pennsylvania, 231 South 34th Street, Philadelphia, PA 19104

[2]Department of Molecular Biophysics and Biochemistry, Yale University, 266 Whitney Avenue, New Haven CT 06511

**Abstract**

Fibrillar deposits of α-Synuclein (αS) are the hallmark of Parkinson's disease. Recent evidence suggests that disease may propagate through cell-to-cell transmission of toxic forms of αS. Relevant to this mechanism, here we report the discovery that αS binds extracellular N-linked glycans. We find that αS binds to proteoliposomes derived from neuronal-lineage cells and that removal of N-linked glycans both decreases binding and alters the conformation of bound αS. Cellular internalization of both monomer and fibrillar αS is specific to neuronal-lineage cells and is reduced dramatically upon cleavage of extracellular N-linked glycans. Our results suggest that interactions with extracellular glycans may play an important role in cellular uptake of αS relevant both to normal proteostasis as well as to transmission of pathogenic αS species.

## Introduction

The pathologies of Parkinson's disease (PD) and related synucleinopathies are characterized by the accumulation of aggregates of the neuronal protein α-Synuclein (αS) (Goedert, 2001). The prevailing hypothesis is that toxicity is mediated by prefibrillar oligomers of αS. Emerging evidence suggests that cell-to-cell transmission of toxic αS species underlies disease progression (Guo and Lee, 2014), although molecular details of this process, including the identity of relevant extracellular inter-action partners, are lacking.

αS is a small, soluble protein that is intrinsically disordered in the cytoplasm (Theillet et al., 2016). It binds peripherally to anionic lipid bilayers through its N-terminal domain, which becomes α-helical upon binding (Dikiy and Eliezer, 2014). The localization of αS to nerve terminals (George et al., 1995, Diao et al., 2013) and to cellular lipid raft domains (Fortin et al., 2004) suggests there are components or properties of cellular membranes which may be important for αS binding and function which may not be fully reproduced by simple lipid mixtures. Indeed,

specific components of the extracellular membrane, including proteins (Mao et al., 2016) and proteoglycans (Ihse et al., 2017), have been identified as having roles in the uptake of pathogenic αS species. These observations motivated our interest in better understanding αS interactions with complex cellular membranes.

**Results**

The lipid and protein composition of giant plasma membrane vesicles (GPMVs) closely resembles the cell plasma membrane (Bauer et al., 2009). GPMVs were harvested from SH-SY5Y and HEK cells and incubated with monomeric N-terminally acetylated αS labeled with Alexa 488 (αS-AL488) (SI) (Trexler and Rhoades, 2012). We used the N-terminally acetylated form of the protein as this modification is ubiquitously present on human-derived protein, both in healthy persons and those with PD (Anderson et al., 2006). αS forms large, bright assemblies on the exterior of the SH-SY5Y GMPVs and causes their clustering (Figures 1A, C – Figure supplement 1A), while it binds only weakly to HEK GPMVs (Figures 1B, C – Figure supplement 1B). This observation suggests a specific extracellular membrane component found in SH-SY5Y cells and absent in HEK cells strongly enhances αS binding.

Both proteins and lipids in the outer plasma membrane are heavily modified by glycosylation (Moremen et al., 2012) and extracellular glycosoaminoglycans (GAGs) have been implicated in the cellular uptake of fibrillar forms of αS (Holmes et al., 2013). Carbohydrates were selectively removed from the extracellular surface of the SH-SY5Y GPMVs by incubation with endoglycosidases. Treatment with peptide-N-glycosidase F (PNGaseF), which cleaves N-linked glycans results in a loss of inhomogenous binding and the bright αS assemblies (Figure 1 – Figure supplement 1C, D), as well as significantly decreasing the amount of bound αS (Figure 1C). By comparison, bright αS assemblies are still observed after treatment with Heparinase I/III, which removes GAGs, or endoglycosidase H (EndoH), which cleaves high mannose N-linked carbohydrates (Figures 1D, E – Figure supplement 1E). Uniform binding of Alexa 488 labeled concanavalin A (conA-AL488), a lectin which binds to α-mannose structures, to SH-SY5Y GPMVs demonstrates that glycoproteins are distributed throughout the GPMV bilayer in the absence of αS (Figure 1 - Figure supplement 1C); the addition of αS results in clustering of conA-stained proteins (Figure 1 - Figure supplement 1F, G). αS appears to induce assembly through binding to and cross-linking multiple membrane glycoproteins, likely observed because GPMVs

lack an intact cytoskeleton which would restrict large-scale rearrangement of plasma membrane proteins.

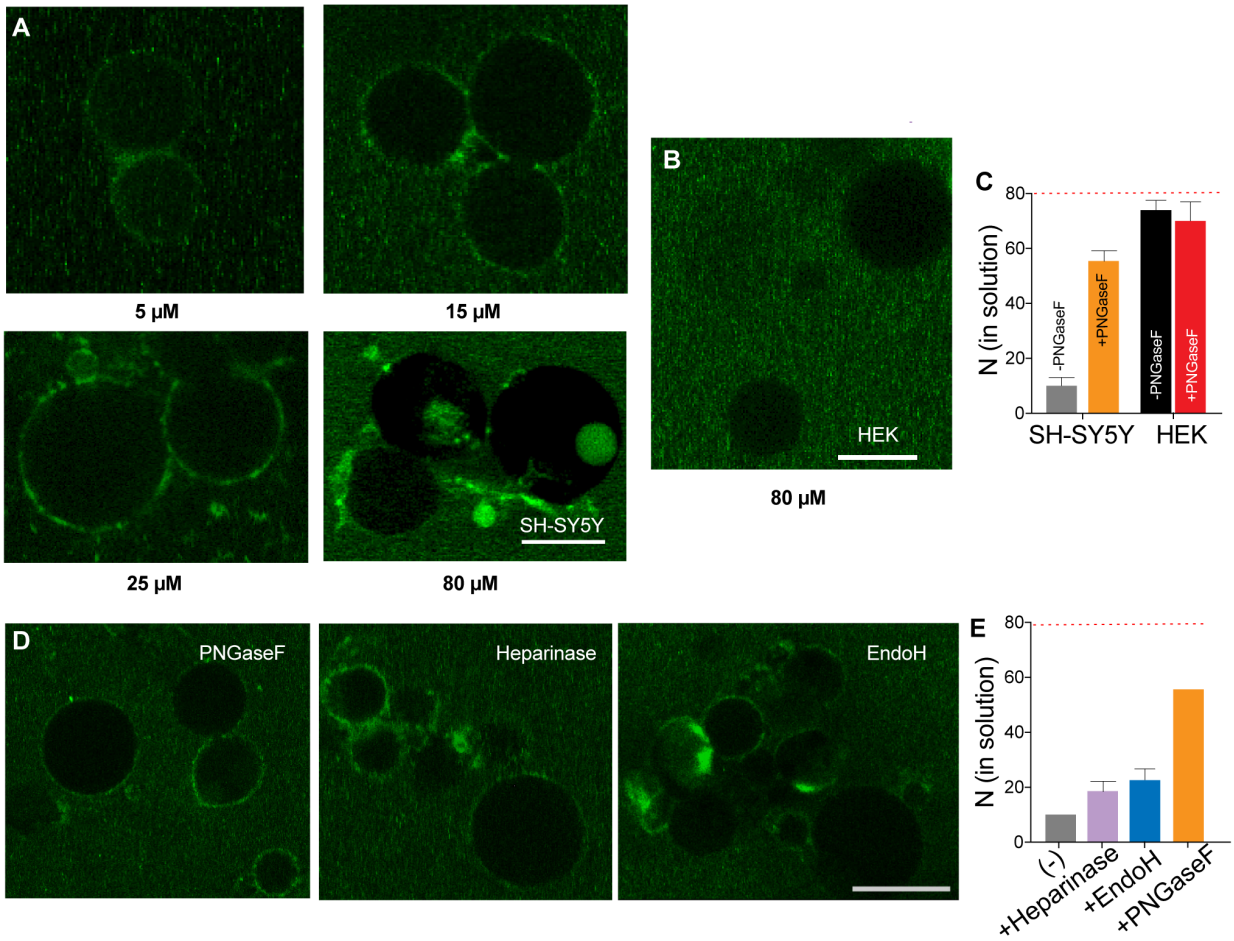


Figure 1. (A) Images of SH-SY5Y GPMVs incubated with 100 nM αS-AL488 and unlabeled αS (concentrations indicated). (B) As in (A) but with HEK GPMVs. (C) Binding of 80 nM αS-AL488 to GPMVs quantified by FCS as loss of protein from solution. The number of molecules (N) in control wells lacking GPMVs is indicated by the red-dashed line. (D) Representative images of SH-SY5Y GPMVs incubated with 100 nM αS-AL488 and 80 μM unlabeled αS after pretreatment of GPMVs with the indicated endoglycosidase. (E) Binding of αS-AL488 to Heparinase- and EndoH-treated SH-SY5Y GPMVs by FCS, as in Figure 1C. Binding +/- PNGaseF from Figure 1C shown for comparison. The data are presented as mean±SD, n=3. Scale bars=20 μm.

The following figure supplement is available for Figure 1:

Figure supplement 1. αS binding to and clustering of SH-SY5Y GPMVs is dependent on N-linked glycans

Intramolecular FRET measurements were made of αS labeled at residues 9 and 72, encompassing much of membrane-binding domain of αS. Mean energy transfer efficiencies ($ET_{eff}$) of αS bound to SH-SY5Y GPMVs, without and with PNGaseF treatment, are 0.43±0.08 and 0.19±0.06, respectively (Figure 2). This lower $ET_{eff}$ is comparable to that of the elongated helix previously observed by single molecule FRET for αS upon binding to synthetic lipid bilayers (Trexler and Rhoades, 2009). αS assumes multiple conformations on even simple synthetic lipid vesicles (Robotta et al., 2011); the relatively broad FRET distributions observed here may reflect a similar degree of conformational heterogeneity. In the absence of complex N-linked glycans, αS binds to GPMVs through interactions with the lipid bilayer resulting in a predominantly extended conformation. In the presence of N-linked glycans, αS binding is enhanced and requires a conformation distinct from the extended, membrane-bound α-helix.

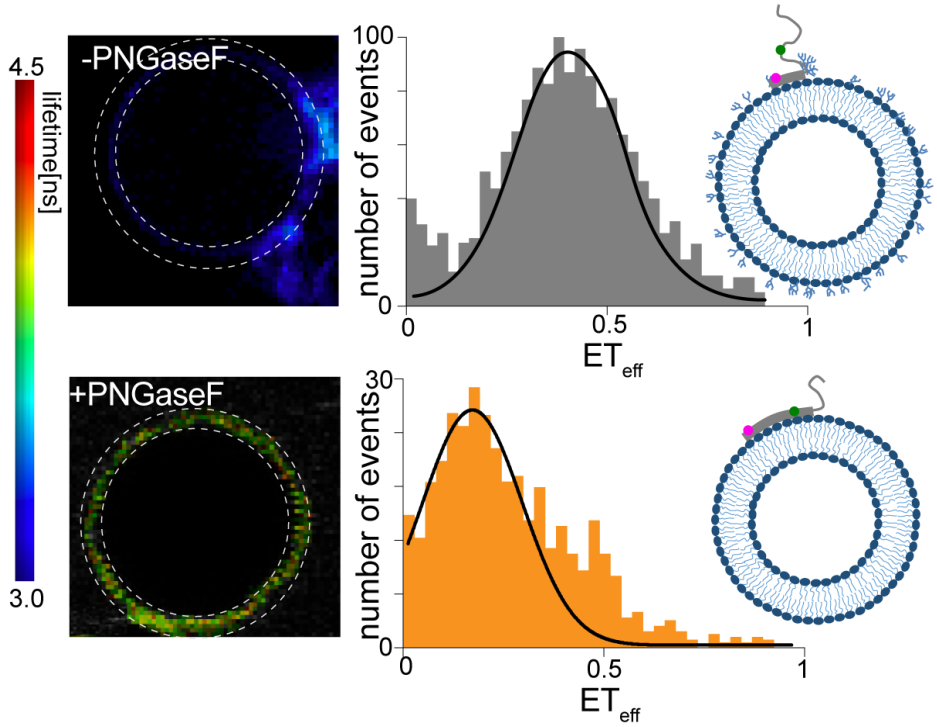


Figure 2 Intramolecular FLIM-FRET measurements of αS bound to untreated or PNGaseF-treated SH-SY5Y GPMVs. Left: Representative image of GPMV, colored by donor fluorophore lifetime shown in the sacle bar. Histogram of $ET_{eff}$ calculated from the images, with Gaussian fits shown. The pixels used to calculate the histograms are indicated by dashed lines on the GPMV images.

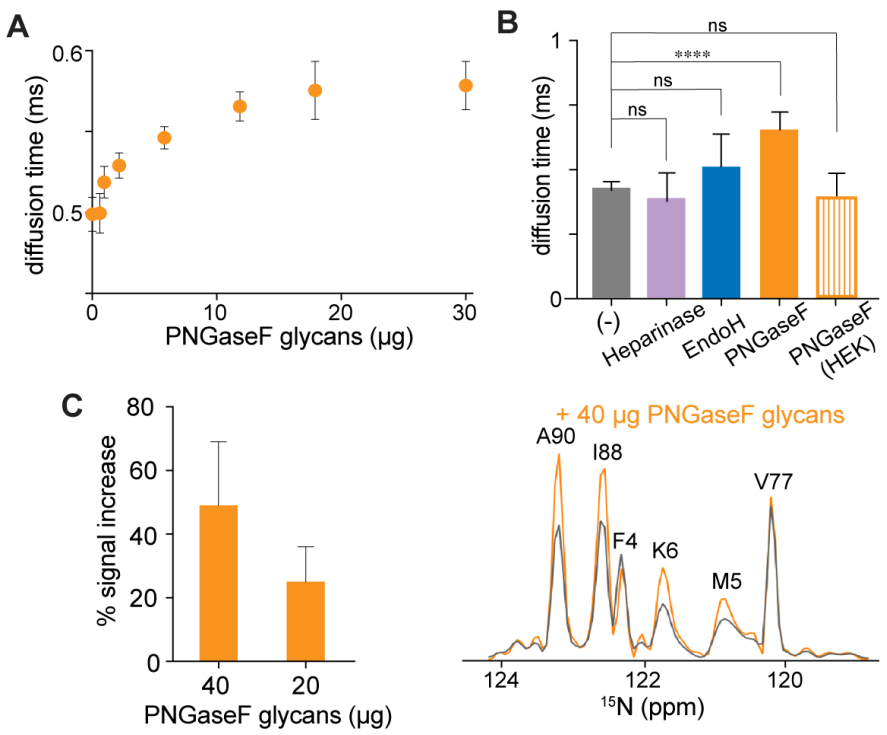


Figure 3 (A) Diffusion time of αS-AL488 (80 nM) as a function of PNGaseF-derived glycan concentration. (B) Comparison of αS-AL488 binding to carbohydrates (30 µg) cleaved by the indicated endoglycosidases. C. (left) Percent increase in peak intensity for selected residues strongly enhanced by glycan binding and (right) cross-sections from $^{15}$N-$^{1}$H HSQC spectra along the nitrogen dimension at 8.15 ppm for αS alone (gray) and in the presence of PNGaseF glycans (orange). For A, B and C, data are presented as mean±S.D., n=3. *P<0.01, **P<0.001 and ***P<0.0001 by the Student's T-Test).

The following figure supplement is available for Figure 3:

Figure supplement 2. αS binding to isolated glycans.

To identify whether αS binding to glycans requires either the associated glycoproteins or a lipid bilayer, binding of αS to glycans in solution was measured by fluorescence correlation spectroscopy (FCS). SH-SY5Y cells were treated with each of the three endoglycosidases above, and the cleaved carbohydrates were isolated. The carbohydrates were titrated into αS-AL488 and the autocorrelation curves were fit to extract the diffusion time and average number of fluorescent molecules, N (Figure 3 - Figure supplement 2A). The diffusion time, which reflects the hydrodynamic size of the diffusing species, of αS increases more than 25% with increasing concentrations of PNGaseF-cleaved glycans, comparable to conA-AL488 (Figures 3A, B – Figure

143 supplement 2B). In contrast to GPMV images, there is no evidence of glycan-mediated assembly
144 of αS in solution (Figure 1 - Figure supplement 2C) which may reflect a difference in αS binding
145 to disperse glycans in solution compared to the relatively high density of glycans on the GPMV
146 surface (Figure 1A). The addition of carbohydrates obtained from EndoH or Heparinase treatment
147 of SH-SY5Y cells or PNGaseF treatment of HEK cells results in minimal changes in the diffusion
148 time of αS by FCS (Figure 3B – Figure supplement 2D). NMR measurements show non-uniform
149 glycan dependent changes in αS peak intensity in the presence of PNGaseF-cleaved glycans
150 (Figures 3C – Figure supplement 2E). By a filtration-based assay, both monomer and pre-formed
151 fibrillar (PFF) αS are found to pull-down PNGaseF-cleaved glycans from solution (Figure 3 -
152 Figure supplement S2F). The specific association of αS with SH-SY5Y-derived complex N-linked
153 glycans both in solution (by FCS, NMR and filtration) and on GPMVs (by imaging and FRET)
154 led us to probe a possible role in cellular internalization of αS.
155 SH-SY5Y and HEK cells were incubated with monomer or PFF αS-AL488 and uptake of
156 protein was monitored (SI). Both forms show time-dependent internalization in SH-SY5Y, but not
157 HEK, cells (Figure 4 – Figure supplement 3A, B). In SH-SY5Y cells, monomer and PFF αS appear
158 as puncta, which co-localize with an endosomal marker (Figure 4 – Figure supplement 3A, C) and
159 uptake is inhibited at 4°C, indicating that active endocytotic pathways is required (Figure 4 - Figure
160 supplement 3D). Clathrin-dependent endocytosis was assessed in SH-SY5Y and HEK cells using
161 transferrin. Both cell lines showed rapid uptake of transferrin, indicating that the αS results are not
162 due to inherent differences in clathrin-dependent endocytosis rates between cell lines (Figure 4 –
163 Figure supplement 3E).
164 Carbohydrate groups were selectively removed from the extracellular surface of SH-SY5Y
165 cells without an impact on clathrin-dependent endocytosis (Figure 4 – Figure supplement 4A, B).
166 After 12 h incubation with αS, a decrease in the number of intracellular puncta relative to untreated
167 cells is observed, both for monomer (WT and mutants) and PFF forms, reflecting a significant
168 decrease in uptake by deglycosylated cells (Figure 4A - Figure supplement 4C, D). Quantification
169 of the kinetics of depletion of monomer and PFF αS from cell media (Figures 4B, C - Figure
170 supplement 4D) as well as of the kinetics of internalization (Figure S4D) confirm that αS uptake
171 is significantly slowed in PNGaseF-treated cells. These observations were validated in
172 cultured primary hippocampal neurons. Both monomer and PFF αS are readily internalized, and
173 removal of extracellular N-linked glycans by PNGaseF results in a 10-fold decrease in the amount

174 of internalized αS (Figure 4D), without causing defects in clathrin-dependent endocytosis (Figure
175 4 – Figure supplement 4B). Under our measurement conditions, neither untreated nor PNGaseF-
176 treated cells show evidence of increased toxicity upon incubation with monomer or PFF αS (Figure
177 4 – Figure supplement 4E).
178

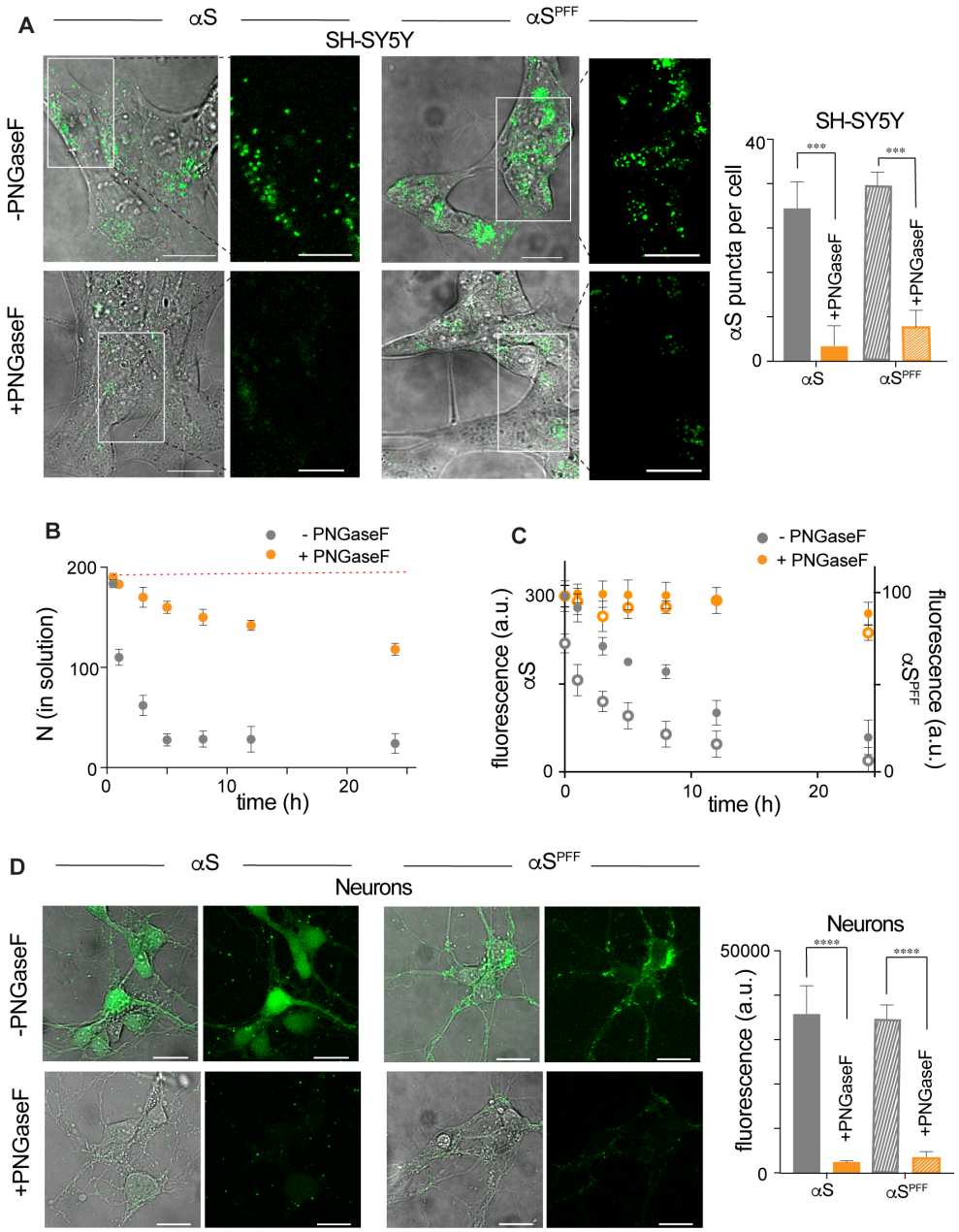


179
180 Figure 4 (A) Uptake of monomer or PFF αS-AL488 by SH-SY5Y cells, -/+ PNGaseF treatment quantified by puncta
181 analysis. (B) Loss of αS-AL488 loss from extracellular medium of SH-SY5Y cells measured by FCS. (C) As in B,
182 but for monomer and PFF αS and quantified by PAGE. (D) Uptake of monomer and PFF αS-AL488 by mouse

183 hippocampal neurons, -/+ PNGaseF treatment quantified by total cellular fluorescence. All αS uptake measurements
184 with 200 nM monomer αS-AL488 or 200 nM $αS^{PFF}$ (monomer units, 20:1 αS:αS-AL488) ; n=100 cells, 3 independent
185 experiments, *P<0.01, **P<0.001 and ***P<0.0001 by the Student's T-Test).
186
187 The following figure supplement is available for Figure 4:
188 Figure supplement 3. Endocytosis of αS.
189 Figure supplement 4. PNGaseF treatment does not disrupt clathrin-mediated endocytosis.
190 Figure supplement 5. N-terminal acetylation of αS is required for its interaction with GPMVs and purified glycans.
191 Figure supplement 6. Heparinase and EndoH treatment of SH-SY5Y cells does not disrupt uptake of monomer αS.
192

193 **Discussion**

194 The data presented in this manuscript provide compelling evidence that αS interacts
195 specifically to extracellular complex, N-linked glycans on SH-SY5Y cells and primary neurons.
196 αS binds to N-linked glycans in solution and on cell-derived proteoliposomes. Uptake of both
197 monomer and PFF αS by SH-SY5Y cells and primary neurons is dependent upon N-linked glycans.
198 While N-linked glycans are present on all mammalian cells, the glycome differs significantly, in
199 the specific sugars and in their distributions, between cell types. The selectivity of αS for N-linked
200 glycans from SH-SY5Y cells and primary neurons over those from HEK cells can be attributed to
201 its ability to differentiate between the specific complex sugars. N-linked glycans have not
202 previously been identified as binding partners of αS, nor as important to its cellular uptake. While
203 internalization of αS PFFs has garnered significant attention because of the potential role in
204 spreading of aggregates in disease (Guo and Lee, 2014) much less attention has been given to
205 monomer αS. However, as αS is secreted even under non-pathogenic conditions (Emmanouilidou
206 et al., 2010), re-uptake of monomer αS by neurons may be important for normal homeostasis.

207 Critical to our discovery is our use of N-terminally acetylated αS. Measurements using the
208 unmodified protein show that it does not bind to complex N-linked glycans on GPMVs or in
209 solution, nor does deglycosylation have an effect on its uptake by SH-SY5Y cells or primary
210 neurons (Figures 1, 2, 3 and 4 – Figure supplement 5). In contrast to other protein modifications,
211 N-terminal acetylation occurs co-translationally and is irreversible (Starheim et al., 2012). It is the
212 predominant modification found on human αS making N-terminally acetylated αS (Anderson et
213 al., 2006) of greater physiological significance than protein lacking this modification. For many

214 proteins, e.g. tropomyosin binding to actin (Hitchcock-DeGregori and Heald, 1987), N-terminal
215 acetylation is required for recognition of binding partners (Drazic et al., 2016), and our current
216 work suggests that this may be true for αS and N-linked glycans. While the fact that both monomer
217 and PFF αS bind to N-linked glycans is initially non-intuitive, high-resolution structures of fibrillar
218 αS show that its N-terminus remains free and disordered (Tuttle et al., 2016). Thus the acetylated
219 N-terminus is accessible in both monomer and PFF αS for glycan-binding. Although here we do
220 not observe a specific role for GAGs in the uptake of monomer, acetylated αS (Figure 4 – Figure
221 supplement 6), prior studies found that they enhance uptake of unmodified fibrillar αS (Ihse et al.,
222 2017, Holmes et al., 2013). Presumably, these interactions are primarily electrostatic, driven by
223 positive residues in the β-sheet core of αS fibers, and thus distinct from the N-terminal driven
224 binding of complex N-linked glycans.

225 One consequence of our observation is that it elicits a reconsideration of putative binding
226 partners for αS. Many of the proteins identified as such contain N-linked glycosylation sites,
227 including glucocerebrosidase (Yap et al., 2011), Rab3b (Cooper et al., 2006) and LAG3 (Mao et
228 al., 2016), although neither the glycosylation state of these proteins, nor the N-terminal acetylation
229 of αS have been explicitly considered in prior studies. For lectins, high affinity binding occurs
230 when the correct cluster of glycans is present and in the correct orientation. Although to our
231 knowledge there are no examples of entirely disordered lectins, one advantage would be con-
232 formational flexibility allowing for recognition and binding of N-linked glycans with non-ideal
233 orientations. It has been shown that both the length and stiffness of the disordered linkers between
234 carbo-hydrate binding domains in enzymes which degrade cell plant-wall polysaccharides are
235 important for orientation of active sites (Rozycki and Cieplak, 2016). While the molecular details
236 of the interaction between αS and complex, N-linked glycans remain to be determined, the results
237 presented here identify a novel class of binding partners for αS with potential implications in
238 normal function and disease transmission.
239

240 **Material and Methods**

241 **αS expression and purification.** αS was expressed in *E. coli* BL21 cells; for N-terminally
242 acetylated αS, BL21 stocks containing the NatB plasmid with orthogonal antibiotic resistance were
243 used. The purification of both acetylated (αS) and unmodified ($\alpha S_{un}$) protein was carried out as
244 previously described [S](Trexler and Rhoades, 2012), with minor modifications. Briefly, two
245 ammonium sulfate cuts were used (0.116 g/mL and 0.244 g/mL) with αS precipitating in the
246 second step. The pellet was resolubilized in Buffer A (25 mM Tris pH 8.0, 20 mM NaCl, 1 mM
247 EDTA) with 1 mM PMSF and dialyzed against Buffer A to remove ammonium sulfate. Dialyzed
248 samples were then loaded to an anion exchange column (GE HiTrap Q HP, 5ml) and eluted with
249 a gradient to 1 M NaCl. αS elutes at approximately 300 mM NaCl. Fractions containing αS were
250 pooled and concentrated using Amicon Ultra concentrators (3000 Da MWCO). Concentrated
251 samples were then loaded to a size exclusion column (GE HiLoad 16/600 Superdex75) and eluted
252 at 0.5 ml/min. Fractions containing αS were again pooled and concentrated, then stored at -80°C.
253 All αS constructs used in this work were checked by MALDI to confirm correct mass and presence
254 of acetylation (Figure supplement 7).

255 For NMR measurements, 15N-labeled αS was grown in E. coli BL21 stocks containing the
256 NatB plasmid in minimal medium (6 g/L $Na_2HPO_4.7H_2O$, 3 g/L $KH_2PO_4$, 0.5 g/L NaCl, 1mM
257 $MgS0_4$, 300 μM $CaCl_2$, 0.5 g/L $^{15}NH_4Cl$) instead of LB medium and purified as described above.

258 **αS labeling.** αS was site-specifically labeled at a single position by introduction of a cysteine at
259 either residue 9 or residue 130. For labeling reactions, freshly purified αS (typically 200–300 μL
260 of ~200 μM protein) was incubated with 1 mM DTT for 30 min at room temperature to reduce the
261 cysteine. The protein solution was passed over two coupled HiTrap Desalting Columns (GE Life
262 Sciences) to remove DTT and buffer exchanged into 20 mM Tris pH 7.4, 50 mM NaCl, 6 M
263 guanidine hydrochloride (GdmCl). The protein was incubated overnight at 4 °C with stirring with
264 a 4x molar excess of Alexa Fluor 488 (AL488) or Alexa Fluor 594 (AL594) maleimide
265 (Invitrogen). The labeled protein was concentrated and buffer exchanged into 20 mM Tris pH 7.4,
266 50 mM NaCl using an Amicon Ultra 3K Concentrator (Millipore), with final removal of unreacted
267 dye and remaining GdmCl by passing again over a set of coupled desalting columns equilibrated
268 with 20 mM Tris pH 7.4, 50 mM NaCl.

269 For dual fluorophore labeling for FRET measurements, cysteines were introduced at
270 residues 9 and 72. The protein was labeled as described above, with the following modifications.
271 The protein was first incubated with donor fluorophore AL488 maleimide at a ratio of protein:dye
272 of 1:0.5 for 2 h at room temperature with stirring. Then, a 4x molar excess of acceptor fluorophore
273 AL594 maleimide (Invitrogen) was added, and the reaction was continued overnight at 4 °C. The
274 labeled protein was separated from unreacted dye as described above. αS labeled at these positions
275 have been extensively studied in our lab; as documented in our previous publications, they do not
276 perturb αS binding to lipid membranes and serve as excellent reporters of different conformations
277 of membrane-associated αS(Trexler and Rhoades, 2009, Middleton and Rhoades, 2010).

278 **Fibril Formation.** αS pre-formed fibrils (PFFs) were prepared as previously described (Volpicelli-
279 Daley et al., 2014). Briefly, 100 μM αS was mixed with 5 μM αS-AL488 in 20 mM Tris pH 7.4
280 and 100 mM NaCl. To induce aggregation, this solution was incubated at 37°C for 5 days with
281 agitation (1500 rpm on an IKA MS3 digital orbital shaker) in parafilm-sealed 1.5 mL Eppendorf
282 tubes to ensure minimal solvent evaporation. The aggregation reaction was analyzed by Congo
283 Red absorbance by diluting 10 μl of the aggregation solution in 140 μl 20 μM Congo Red. The
284 mature fibrils were then pelleted by centrifugation (13,200 rpm for 90 mins at 4°C) and the
285 supernatant removed. Fibers were resuspended in an equal volume (relative to supernatant) of 20
286 mM Tris pH 7.4, 100 mM NaCl. Mature fibers were subsequently fragmented on ice using a
287 sonicator (Diagenode Biorupter™ UCD-300 bath sonicator set to high, 30s sonication followed
288 by a delay period of 30s, 10 min total) to form PFFs.

289 **Assessment of fibrillar material** TEM and PAGE were used to characterize fibrillar αS (Figure
290 supplement 7). For TEM, 10 μL of aggregated protein samples (from both before and after
291 sonication) were incubated on TEM grids (400-mesh Formvar carbon coated copper, Electron
292 Microscopy Sciences) for 1–2 minutes. Sample solution was wicked with filter paper and grid was
293 washed with water to remove any excess material and improve background contrast. Grids were
294 then incubated with 1% (w/v) aqueous uranyl acetate (UA) solution (10 μL) for 30–60 s. Excess
295 UA was wicked away with filter paper and grids were air dried. TEM images were collected using
296 a JOEL JEM 1011 TEM (operating voltage 100 kV) equipped with a charge-coupled device
297 camera (ORIUS 832. 10W; Gatan). For PAGE, aggregated protein solutions were centrifiuged to
298 pellet the aggregated material. The upernatant was removed and pellet was resuspended in the

299 starting volume of buffer. Both supernatant and resuspended pellet (20 μL) were loaded on a 4-
300 12% polyacrylamide gel. Gels were imaged using a Typhoon FLA7000 gel imager (GE Life
301 Sciences) using Coomassie stain mode.

302

303 **Cell culture.** Human neuroblastoma (SH-SY5Y) and human embryonic kidney 293T (HEK) cells
304 were grown at 37 °C under a humidified atmosphere of 5% $CO_2$. The SH-SY5Y cells were cultured
305 in Dulbecco's Modified Eagle's Medium (DMEM) plus 10% fetal bovine serum, 50 U/ml penicillin
306 and 50 μg/ml streptomycin. The HEK cells were cultured in DMEM supplemented with 10% FBS,
307 2mM L-glutamine and 100 units/ml penicillin-streptomycin.

308 Cells were passaged upon reaching ~95% confluence (0.05% Trypsin-EDTA, Life
309 Technologies), propagated and/or used in experiments**.** Cells used in experiments were pelleted
310 and resuspended in fresh media lacking Trypsin-EDTA.

311 **Primary Neuronal Culture**. Primary neuronal cultures were prepared from E15-E17 embryos of
312 CD1 mice. All procedures were performed according to the NIH Guide for the Care and Use of
313 Experimental Animals and were approved by the University of Pennsylvania Institutional Animal
314 Care and Use Committee (IACUC). Dissociated hippocampal neurons were plated onto sterile,
315 poly-D-lysine coated on IBIDI chambers at 200,000 cells/coverslip for live cell imaging and were
316 allowed to mature for 5 days in complete neuronal medium (Neurobasal without phenol red
317 (Thermo Fisher), 5% B27 supplement (Thermo Fisher)). Medium was partially exchanged every
318 3-4 days.

319 **Giant Plasma Membrane Vesicles.** Giant plasma membrane vesicles (GPMVs) are blebs
320 obtained directly form the cell plasma membrane that contain lipid bilayers and the embedded
321 membrane proteins, but lack the other biological components of the cell [S](Bauer et al., 2009).
322 GPMVs were isolated from SH-SY5Y and HEK cells according to established methods [S](Sezgin
323 et al., 2012)**.** Briefly, cells were plated in 25 $cm^2$ culture flasks and cultured for 48 h**,** washed with
324 GPMV buffer (10 mM HEPES, 150 mM NaCl, 2 mM $CaCl_2$, pH 7.4) twice and then exposed to
325 25 mM formaldehyde and 2 mM DTT for 2 h to induce blebbing**.** To reduce the content of DTT,
326 GPMVs were dialyzed in GPMV buffer prior to use in experiments. GPMVs were also created
327 using *N*-ethylmaleimide as the blebbing reagent, with comparable results. The phospholipid
328 content of final material was measured by total phosphate assay.

329 **Phosphate assay.** Lipid concentrations for GPMV preparations were estimated by measuring total
330 phosphate, assuming that all measured phosphate is from phospholipids, and that all lipids are
331 phospholipids. This is a practical assumption designed to ensure reproducibility.

332 **Enzymatic cleavage of carbohydrates.** For cleavage of carbohydrates from GPMVs,
333 endoglycosidases were added to the GPMVs in GPMV buffer at concentrations recommended by
334 the manufacturers (PNGaseF - 5,000 units/ml; EndoH - 2500 units; heparinaseI/II - 2500 units)
335 and incubated at 37°C for 6 h. PNGaseF was tagged with a chitin binding domain (Remove-IT
336 PNGaseF, New England Biolabs, MA, USA). For the images shown in this manuscript, the enzyme
337 was removed by incubation of GPMVs with 50 μl of chitin binding magnetic beads. However,
338 control experiments were conducted without removal of PNGaseF and found to be comparable.
339 Cleavage of N-linked glycans by PNGaseF was confirmed by comparing images of GPMVs +/-
340 PNGaseF treatment after incubation with 50 nM concanavalin A (conA), a lectin which binds to
341 binding to α-D-mannose and α-D-glucose moieties, or wheat germ agglutinin, a lectin which binds
342 to N-acetyl-D-glucosamine and sialic acid. A significant decrease in the amount of both proteins
343 is observed in these images (Figure supplement 1).

344 For cleavage of carbohydrates from cells, cells were first plated for 42 h. After 42 h, media
345 was removed from cells and replaced with FBS-free media complimented with the
346 endoglycosidase (PNGaseF - 5,000 units/ml; EndoH - 2500 units; heparinaseI/II - 2500 units). The
347 cells were incubated at 37°C under a humidified atmosphere of 5% $CO_2$ for an additional 6 h. The
348 media was then removed and replaced with cell growth media prior to the addition of αS. Cleavage
349 of N-linked glycans from cells was confirmed by comparing images +/- PNGAseF treatment after
350 incubation with 50 nM conA-AL488, showing a significant reduction in the amount of conA bound
351 (Figure supplement 4A).

352 To ensure that PNGaseF is removed from GPMVs or cells after incubation (and therefore
353 does not remain associated with either, blocking potential αS binding sites), we compared the
354 amount of PNGaseF added to either GPMVs or cells with that removed after incubation. PNGaseF
355 (5,000 units/ml) containing a chitin domain was added to chambers containing either GPMVs or
356 cells and incubated at 37°C for 6 h, as for the experiments described above. After incubation, the
357 buffer or media containing PNGaseF was removed incubated with chitin magnetic beads to isolate
358 and concentrate the enzyme. Blank chambers containing only PNGaseF in buffer or media were

359 subjected to the same treatment. 20 uL of each sample was run on a 4-12% polyacrylamide gels
360 and stained with Coomassie blue. Gels were imaged using a Typhoon FLA7000 gel imager (GE
361 Life Sciences) using Coomassie stain mode. The gels indicate that essentially all of the enzyme is
362 removed (Figure supplement 8).

363 **Quantification of carbohydrates.** Concentrations of carbohydrates isolated from GPMVs or cells
364 were quantified by using the Total Carbohydrate Quantification Assay Kit (Abcam, MA, USA)
365 following the manufacturer's instructions. Briefly, the carbohydrates are first hydrolyzed to
366 monomer sugar units and then converted to furfural or hydrofurfural. These compounds are
367 converted to chromogens, which can be detected by absorbance at 490 nm. Glucose was used to
368 generate a standard curve for calculated of the total carbohydrate concentration of the samples.

369 **αS-captured carbohydrate pulldown assay.** Carbohydrates cleaved and isolated from GPMVs
370 (50 μg) were incubated with 100 μM αS in 100 μL 10 mM HEPES, 150 mM NaCl, 2 mM $CaCl_2$,
371 pH 7.4 for 1 h at room temperature. Binding reaction mixes were transferred to Amicon Ultra
372 (3000 Da MWCO) centrifugal concentration devices that had been washed with 500 μL deionized
373 water. The concentrators were centrifuged for 5 min at 4200 rpm and the filtrates collected. The
374 flow-through contains carbohydrates that did not bind αS and thus were not retained in the chamber
375 of the concentrator. The amount of carbohydrate in the flow-through was quantified by the total
376 carbohydrate assay as described above. The fraction of carbohydrate bound and retained by αS
377 ($C_{captured}$) was calculated relative to the starting concentration (50 μg) of the carbohydrate
378 mixture, using;

379 $$C_{captured} = C_{total} - C_{flow-through} \quad \text{(eq. 1)}$$

380

381 Where $C_{total}$ corresponds to the absorption of the starting stock concentration of carbohydrates
382 used and $C_{flow-through}$ is the absorption of the flow-through.

383 Samples containing αS with no glycans or conA with 50 μg glycans were used as negative
384 and positive controls, respectively. As expected, no signal at 490 nm was detected for the αS-only
385 sample; the conA results are shown in Figure supplement 2. The absorbance of flow-through at
386 280 nm was measured, confirming that all protein was retained in the concentrator and could not
387 be detected in the flow-through.

388 **Cell imaging and analysis.** All cell imaging was carried out by confocal fluorescence microscopy
389 using an Olympus FV3000 scanning system configured on a IX83 inverted microscope platform
390 with a 60x Plan-Apo/1.1-NA water-immersion objective with DIC capability (Olympus, Tokyo,
391 Japan). For all experiments the gain setting for the blue channel was kept constant from sample to
392 sample (excitation 488 nm, emission BP 500-540 nm). For detection of αS-AL594, the green
393 channel was used (excitation 561 nm, emission BP 570-620 nm). Images were obtained in 8-well
394 ibidi chambers (μ-Slide, 8-well glass bottom, ibidi GmbH, Germany) coated with Poly-D-lysine
395 and were seeded with 20000-25000 cells/well. Cells were cultured for 48 h after passage before
396 beginning experiments. For cellular uptake experiments, 200 nM αS-AL488 was incubated with
397 cells for 0 to 24 h before acquiring images. For experiments using deglycosylated cells, cells were
398 pretreated with the tested endoglycosidase for 6 h as described above prior to addition of protein.
399 For colocalization with lysosomes, cells were treated with 75 nM Lysotracker Deep Red (Life
400 Technologies) for 1 h prior to imaging. For all experiments, the gain setting for each channel was
401 kept constant from sample to sample.

402 Image acquisition and processing were performed with the software accompanying the
403 FV3000 microscope and Image J software (Schneider et al., 2012). For SH-SY5Y cells,
404 internalized αS was quantified either by analysis of the punctate structures in the cells or by the
405 total cellular fluorescence; for primary neurons, internalized αS was quantified by total cellular
406 fluorescence. For total cellular fluorescence, the integrated fluorescence intensity of the cells is
407 calculated and reported. Cellular puncta were analyzed using the Image J particle analysis plug-
408 in. This algorithm detects puncta through a user-defined threshold and counts the number of puncta
409 that meet or exceed the threshold. The threshold was initially defined by manual identification and
410 averaging of a subset of puncta. Colocalization with lysosomes was computed by obtaining a
411 Pearson coeffieient using the ImageJ plugin for co-localization (Coloc_2).

412 **Endocytosis inhibition.** For inhibition of exocytosis experiments, monomer αS-AL488 (200 nM)
413 or PFFs (200 nM in monomer units, 20:1 αS:αS-AL488) was initially incubated with cells for 30
414 minutes at 4°C. Control cells were moved to 37°C while the endocytosis inhibited cells were
415 incubated at 4°C for another 4 h before acquiring images. For all experiments, the gain setting for
416 each channel was kept constant from sample to sample. Image acquisition and processing were

417 achieved using the software accompanying the FV3000 microscope and Image J software
418 (Schneider et al., 2012).

419 **GPMV imaging and analysis.** All GPMV images were carried using a PicoQuant MicroTime 200
420 time-resolved fluorescence system based on an inverted Olympus IX73 microscope (Olympus,
421 Tokyo, Japan) with a 60x Plan-Apo/1.4-NA water-immersion objective using a 482 nm excitation
422 laser and a frame size of 512 × 512 pixels. Images acquired with this instrument were in lifetime
423 mode but were integrated to obtain intensity based images comparable to typical confocal images.
424 This instrument has the advantage of very sensitive avalanche photodiode detectors (SPADs) that
425 are capable at detecting nM concentrations of protein. Fluorescence intensities were analyzed by
426 via the lifetime mode (both intensity and FRET images) using SymPhoTime 64 (PicoQuant). The
427 intensity of images was then adjusted on ImageJ analysis program (Schneider et al., 2012).

428 For FLIM-FRET experiments, measurements were made of donor-only and donor-acceptor
429 labeled proteins. SPAD signals were processed with the TimeHarp 300 photon counting board and
430 analyzed with the SymPhoTime 64 software (PicoQuant) taking into account the instrument
431 response function to allow consideration of short lifetime components with a high accuracy. FLIM
432 images were acquired for 180 s, with a pixel integration time of 40 μs per pixel and an average
433 photon count rate of 10000–30000 counts per second. Regions of interest of the GPMV membrane
434 were selected from FLIM images and fluorescent lifetimes were obtained from TCSPC decay
435 curves fitted by an exponential equation using the SymPhoTime 64 software. Fitting of the
436 fluorescence images was then performed pixel wise with a single exponential model on all pixels
437 above an intensity threshold of 200 photons. By characterizing donor lifetime in the absence and
438 presence of acceptor, FRET efficiency ($ET_{eff}$) can be calculated from:

439 $$ET_{eff} = 1 - \frac{\tau_{DA}}{\tau_D} \qquad \text{(eq. 2)}$$

440 where $\tau_{DA}$ and $\tau_D$ and are the donor excited state lifetime in the presence and absence of acceptor.
441 Six FLIM images were recorded for each of three biological repeats per condition. The histograms
442 shown in Figure 2 represents $ET_{eff}$ values for selected pixels from equatorial sections of the
443 GPMVs as indicated on the images to their left. The histograms were fit with a Gaussian function
444 to extract the mean $ET_{eff.}$

445 Images were obtained in 8-well NUNC chambers (Thermo Scientific, Rochester, NY,
446 USA) coated with Poly-D-lysine, containing 250 µl of GMPV at 5 µM phospholipid concentration
447 and 80 nM of αS labeled with Alexa 488. For all experiments using these chambers, the chambers
448 were passivated by polylysine-conjugated PEG treatment to prevent any nonspecific absorption to
449 the chamber surfaces (Middleton and Rhoades, 2010).

450 **Fluorescence correlation spectroscopy (FCS).** Fluorescence correlation spectroscopy (FCS)
451 measurements were carried out on a lab-built instrument, as described previously (Trexler and
452 Rhoades, 2009). A 488-nm-wavelength laser was adjusted to 5 µW prior to entering the
453 microscope. Fluorescence emission was collected through the objective and separated from laser
454 excitation using a Z488RDC Long-Pass Dichroic and an HQ600/200M Band-Pass Filter
455 (Chroma). The fluorescence emission was focused into the aperture of a 50-µm-diameter optical
456 aperture fiber (OzOptics) directly coupled to an avalanche photodiode. A digital correlator
457 (Flex03LQ-12; Correlator.com) was used to generate the autocorrelation curves. For each
458 experiment, 30 autocorrelation curves of 10 s each were acquired and averaged together to obtain
459 statistical variations. These average autocorrelation curves were then fit to a function for single
460 fluorescent particles undergoing Brownian motion in a 3D Gaussian volume weighted by the
461 inverse square of the SD:

462 $$G(\tau) = \frac{1}{\mathrm{N}} \times \frac{1}{1+\frac{\tau}{\tau_D}} \times \sqrt{\frac{1}{1+\frac{s^2\tau}{\tau_D}}} \qquad (\mathrm{eq.}\,3)$$

463 where G(τ) is the autocorrelation function for translational diffusion as a function of time τ, N is
464 the average number of fluorescent molecules in the laser focal volume, and $\tau_D$ is the translational
465 diffusion time of the particles. The structure factor, s, is the ratio of the radial to axial dimensions
466 of the focal volume and was obtained from a calibration procedure using Alexa 488 hydrazide dye
467 solutions (s = 0.2) and fixed for all subsequent fitting. Several datasets of autocorrelation curves
468 obtained in the presence of carbohydrates were analyzed considering a single component system.
469 For carbohydrate binding, both the diffusion time, $\tau_D$, (Figures 3A, 3B and Figure supplement 2B,
470 2D, 5C and 9) and the number of molecules, N, (Figures 1C, 1E, 4B and Figure supplement 2C,
471 3E, 5B, 5D and 9) were analyzed.

472 **GPMV binding and cellular uptake by FCS.** FCS was used to monitor αS both binding to
473 GPMVs and uptake by cells. FCS measurements were made on the instrument described above.

474 For GPMV binding, experiments were performed in 8-well NUNC chambers (Thermo Scientific,
475 Rochester, NY, USA) containing 250 µl of GMPV at 5 µM phospholipid concentration. The laser
476 focal volume was located to a height of 100 µm from the bottom surface of the wells, above all
477 GMPVs. αS labeled with Alexa 488 (80 nM) was added to wells with GPMVs and the
478 autocorrelation measurements were taken immediately and after 60 minutes. Each curve was
479 integrated for 30 s, repeated 10 times and data was analyzed as described above. Binding was
480 quantified by measuring the change in the number of molecules, N, of fluorescently labeled αS
481 present in the solution surrounding the GMPVs relative to the starting concentration. There was
482 no change in the diffusion time of the αS that remained in the cell media over this time course,
483 evidence that protein is stable and the fluorophore intact (Figure supplement 9).

484 For cell uptake experiments, cells were plated in phenol red-free medium in 8-well ibidi
485 chambers (µ-Slide, 8-well glass bottom, ibidi GmbH, Germany) coated with Poly-D-lysine wells
486 and cultured for 48 h prior to measurements. Control wells contained the same volume of media
487 without cells; these control for non-specific adsorption of protein to the well surfaces. αS-AL488
488 (200 nM) was added to the wells at the start of the experiment, and the autocorrelation curves were
489 taken in the medium well above the cells, at a height of 100 µm from the bottom surface of the
490 wells. The curves were collected at regular intervals, over a period ranging from 2 to 24 h, and
491 each autocorrelation curve integrated for 30 s, repeated 10 times. Data were analyzed as described
492 above. Cellular uptake was assessed by measuring the change in the number of molecules of
493 fluorescently labeled αS present in the media surrounding the cells relative to the starting
494 concentration. In between measurements, the chambers were returned to the incubators to maintain
495 the temperature in the wells at 37°C. As a negative control for both the GPMV binding and cell
496 uptake studies, GPMVs or cells were incubated with 80 nM eGFP. There was no evidence of eGFP
497 binding to the GPMVs nor of internalization by SH-SY5Y cells (Figure supplement 10).

498 **Cellular uptake by PAGE**. As an orthogonal approach to the FCS and imaging approached
499 described above, uptake of both monomer and PFF αS were quantified by PAGE. SH-SY5Y cells
500 were incubated with 200 nM αS, as described above for FCS uptake experiments. After incubation
501 for the desired time (1, 3, 5, 8, 12, or 24 h) the media was removed from cells and stored at 4°C.
502 After all samples were collected, 20 µl of each sample were run on a 4-12% polyacrylamide gel.

503 To quantify the amount of protein internalized, an identical set of experiments was carried
504 out, with modifications as described in the following. For each time point, transferrin-AL488 (100
505 nM) was added 30 min prior to the due time of the time point to serve as a loading control. At the
506 desired time points, the cells were detached from the wells by 0.05% Trypsin-EDTA (Life
507 Technologies), pelleted and lysed in 250 μl RIPA lysis buffer (Thermo Fisher). Cell lysates (20 μl
508 of stock) were run on PAGE gels. Cell lysates (20 μl) were run on 4-12% polyacrylamide gels.

509 Gels of both extracellular and internalized αS were imaged using a Typhoon FLA7000 gel
510 imager (GE Life Sciences) using fluorescent imaging mode to detect αS-AL488 or transferrin-
511 AL488. Image J was used to quantify the bands.

512 **Statistical analysis.** Data are expressed as the mean ± SD, and were examined by a one-way
513 analysis of variance (n = 3). More than three experiments were performed and similar results were
514 obtained. P values less than 0.05 were considered to be significant.

515 **Trypan Blue Quenching.** Trypan blue solution 0.4% (Thermo Fisher) and fresh neurobasal
516 without phenol red, B27, or antibiotic supplementation were equilibrated at 37°C. A 10X dilution
517 of trypan blue was prepared freshly in the warmed neurobasal media. The trypan blue solution was
518 then added to cells dropwise and incubated at 37°C for an hour prior to imaging. Trypan Blue
519 quenching was performed for all imaging experiments performed using PFFs and when monomer
520 protein was introduced in experiments utilizing primary neurons. Trypan Blue quenching was used
521 eliminate signal from extracellular material allowing the fluorescence quantification of
522 intracellular fluorescence signal.

523 **Nuclear Magnetic Resonance.** $^{1}$H-$^{15}$N HSQC NMR titrations were carried out at 25°C using
524 Varian 600 MHz or Agilent 800 MHz spectrometers equipped with room temperature probes. A
525 uniformly labeled $^{15}$N-αS solution was added to either N-linked glycans obtained by PNGaseF
526 cleavage from SH-SY5Y cells or commercially available mono- or trisaccharides at the
527 concentrations indicated in Figures 4 and S2E in GPMV buffer (10 mM HEPES, 150 mM NaCl,
528 2 mM CaCl2, pH 7.4, 10% $D_2O$; final concentration of $^{15}$N-αS was 350 μM). HSQC spectra were
529 collected with VnmrJ software using built-in pulse sequence including WATERGATE solvent
530 suppression and analyzed with Mnova software suite (Mestrelab). Standard parameters for zero-
531 filling, apodization and baseline correction were applied. $^{1}$H chemical shifts were referenced using

532 water resonance and $^{15}N$ chemical shifts were referenced indirectly based on gyromagnetic ratios
533 of respective nuclei. Previously assigned αS backbone resonances were used(Kang et al., 2011).
534 Binding to the PNGaseF derived glycans results in non-uniform peak intensity increases
535 throughout the sequence of αS. For analysis, 10 peaks showing large increases and 10 peaks
536 showing small or no increases were selected to roughly cover the entire sequence. The same
537 residues were used for each analyzed dataset. For each set of peaks, the relative magnitude of
538 increase (as compared to αS in solution without glycans) expressed as a percentage was calculated
539 and averaged. A difference between two numbers is reported in Figure 3C of the manuscript. The
540 same calculation was carried out for the mono- and tri-saccharides, which do not bind to αS, shown
541 in Figure supplement 2E.
542
543 **Acknowledgments**
544 This research was supported by NIH R01 NS079955 and the Michael J. Fox Foundation (to E.R.).
545 We thank T. Baumgart for use of his confocal microscope and V. M.-Y. Lee for use of her
546 sonicator. We also thank M. Maronski of the Neuron Cell Core in the The Mahoney Institute for
547 Neurosciences in the Perlman School of Medicine at the University of Pennsylvania for
548 hippocampal neuron preparation and R. Jin for providing the vesicle schematic adapted for Figure
549 2. All data are available from authors by request.
550
551 **Competing interests**
552 The authors declare that no competing interests exist.
553

554 **References**


555 ANDERSON, J. P., WALKER, D. E., GOLDSTEIN, J. M., DE LAAT, R., BANDUCCI, K., CACCAVELLO, R.
556 J., BARBOUR, R., HUANG, J., KLING, K., LEE, M., DIEP, L., KEIM, P. S., SHEN, X., CHATAWAY,
557 T., SCHLOSSMACHER, M. G., SEUBERT, P., SCHENK, D., SINHA, S., GAI, W. P. & CHILCOTE,
558 T. J. 2006. Phosphorylation of Ser-129 is the dominant pathological modification of alpha-
559 synuclein in familial and sporadic Lewy body disease. *J Biol Chem,* 281**,** 29739-52,
560 10.1074/jbc.M600933200.
561 BAUER, B., DAVIDSON, M. & ORWAR, O. 2009. Proteomic analysis of plasma membrane vesicles.
562 *Angew Chem Int Ed Engl,* 48**,** 1656-9, 10.1002/anie.200803898.
563 COOPER, A. A., GITLER, A. D., CASHIKAR, A., HAYNES, C. M., HILL, K. J., BHULLAR, B., LIU, K., XU,
564 K., STRATHEARN, K. E., LIU, F., CAO, S., CALDWELL, K. A., CALDWELL, G. A., MARSISCHKY,
565 G., KOLODNER, R. D., LABAER, J., ROCHET, J. C., BONINI, N. M. & LINDQUIST, S. 2006.
566 Alpha-synuclein blocks ER-Golgi traffic and Rab1 rescues neuron loss in Parkinson's
567 models. *Science,* 313**,** 324-8, 10.1126/science.1129462.
568 DIAO, J., BURRE, J., VIVONA, S., CIPRIANO, D. J., SHARMA, M., KYOUNG, M., SUDHOF, T. C. &
569 BRUNGER, A. T. 2013. Native alpha-synuclein induces clustering of synaptic-vesicle mimics
570 via binding to phospholipids and synaptobrevin-2/VAMP2. *Elife,* 2**,** e00592,
571 10.7554/eLife.00592.
572 DIKIY, I. & ELIEZER, D. 2014. N-terminal acetylation stabilizes N-terminal helicity in lipid- and
573 micelle-bound alpha-synuclein and increases its affinity for physiological membranes. *J*
574 *Biol Chem,* 289**,** 3652-65, 10.1074/jbc.M113.512459.
575 DRAZIC, A., MYKLEBUST, L. M., REE, R. & ARNESEN, T. 2016. The world of protein acetylation.
576 *Biochim Biophys Acta,* 1864**,** 1372-401, 10.1016/j.bbapap.2016.06.007.
577 EMMANOUILIDOU, E., MELACHROINOU, K., ROUMELIOTIS, T., GARBIS, S. D., NTZOUNI, M.,
578 MARGARITIS, L. H., STEFANIS, L. & VEKRELLIS, K. 2010. Cell-produced alpha-synuclein is
579 secreted in a calcium-dependent manner by exosomes and impacts neuronal survival. *J*
580 *Neurosci,* 30**,** 6838-51, 10.1523/JNEUROSCI.5699-09.2010.
581 FORTIN, D. L., TROYER, M. D., NAKAMURA, K., KUBO, S., ANTHONY, M. D. & EDWARDS, R. H. 2004.
582 Lipid rafts mediate the synaptic localization of alpha-synuclein. *J Neurosci,* 24**,** 6715-23,
583 10.1523/JNEUROSCI.1594-04.2004.
584 GEORGE, J. M., JIN, H., WOODS, W. S. & CLAYTON, D. F. 1995. Characterization of a novel protein
585 regulated during the critical period for song learning in the zebra finch. *Neuron,* 15**,** 361-
586 72.
587 GOEDERT, M. 2001. Alpha-synuclein and neurodegenerative diseases. *Nat Rev Neurosci,* 2**,** 492-
588 501, 10.1038/35081564.
589 GUO, J. L. & LEE, V. M. 2014. Cell-to-cell transmission of pathogenic proteins in
590 neurodegenerative diseases. *Nat Med,* 20**,** 130-8, 10.1038/nm.3457.
591 HITCHCOCK-DEGREGORI, S. E. & HEALD, R. W. 1987. Altered actin and troponin binding of amino-
592 terminal variants of chicken striated muscle alpha-tropomyosin expressed in Escherichia
593 coli. *J Biol Chem,* 262**,** 9730-5.
594 HOLMES, B. B., DEVOS, S. L., KFOURY, N., LI, M., JACKS, R., YANAMANDRA, K., OUIDJA, M. O.,
595 BRODSKY, F. M., MARASA, J., BAGCHI, D. P., KOTZBAUER, P. T., MILLER, T. M., PAPY-
596 GARCIA, D. & DIAMOND, M. I. 2013. Heparan sulfate proteoglycans mediate

597 internalization and propagation of specific proteopathic seeds. *Proc Natl Acad Sci U S A,*
598 110**,** E3138-47, 10.1073/pnas.1301440110.
599 IHSE, E., YAMAKADO, H., VAN WIJK, X. M., LAWRENCE, R., ESKO, J. D. & MASLIAH, E. 2017. Cellular
600 internalization of alpha-synuclein aggregates by cell surface heparan sulfate depends on
601 aggregate conformation and cell type. *Sci Rep,* 7**,** 9008, 10.1038/s41598-017-08720-5.
602 KANG, L., WU, K. P., VENDRUSCOLO, M. & BAUM, J. 2011. The A53T mutation is key in defining
603 the differences in the aggregation kinetics of human and mouse alpha-synuclein. *J Am*
604 *Chem Soc,* 133**,** 13465-70, 10.1021/ja203979j.
605 MAO, X., OU, M. T., KARUPPAGOUNDER, S. S., KAM, T. I., YIN, X., XIONG, Y., GE, P., UMANAH, G.
606 E., BRAHMACHARI, S., SHIN, J. H., KANG, H. C., ZHANG, J., XU, J., CHEN, R., PARK, H.,
607 ANDRABI, S. A., KANG, S. U., GONCALVES, R. A., LIANG, Y., ZHANG, S., QI, C., LAM, S.,
608 KEILER, J. A., TYSON, J., KIM, D., PANICKER, N., YUN, S. P., WORKMAN, C. J., VIGNALI, D.
609 A., DAWSON, V. L., KO, H. S. & DAWSON, T. M. 2016. Pathological alpha-synuclein
610 transmission initiated by binding lymphocyte-activation gene 3. *Science,* 353,
611 10.1126/science.aah3374.
612 MIDDLETON, E. R. & RHOADES, E. 2010. Effects of curvature and composition on alpha-synuclein
613 binding to lipid vesicles. *Biophys J,* 99**,** 2279-88, 10.1016/j.bpj.2010.07.056.
614 MOREMEN, K. W., TIEMEYER, M. & NAIRN, A. V. 2012. Vertebrate protein glycosylation: diversity,
615 synthesis and function. *Nat Rev Mol Cell Biol,* 13**,** 448-62, 10.1038/nrm3383.
616 ROBOTTA, M., BRAUN, P., VAN ROOIJEN, B., SUBRAMANIAM, V., HUBER, M. & DRESCHER, M.
617 2011. Direct evidence of coexisting horseshoe and extended helix conformations of
618 membrane-bound alpha-synuclein. *Chemphyschem,* 12**,** 267-9, 10.1002/cphc.201000815.
619 ROZYCKI, B. & CIEPLAK, M. 2016. Stiffness of the C-terminal disordered linker affects the
620 geometry of the active site in endoglucanase Cel8A. *Mol Biosyst,* 12**,** 3589-3599,
621 10.1039/c6mb00606j.
622 SCHNEIDER, C. A., RASBAND, W. S. & ELICEIRI, K. W. 2012. NIH Image to ImageJ: 25 years of image
623 analysis. *Nat Methods,* 9**,** 671-5.
624 SEZGIN, E., KAISER, H. J., BAUMGART, T., SCHWILLE, P., SIMONS, K. & LEVENTAL, I. 2012.
625 Elucidating membrane structure and protein behavior using giant plasma membrane
626 vesicles. *Nat Protoc,* 7**,** 1042-51, 10.1038/nprot.2012.059.
627 STARHEIM, K. K., GEVAERT, K. & ARNESEN, T. 2012. Protein N-terminal acetyltransferases: when
628 the start matters. *Trends Biochem Sci,* 37**,** 152-61, 10.1016/j.tibs.2012.02.003.
629 THEILLET, F. X., BINOLFI, A., BEKEI, B., MARTORANA, A., ROSE, H. M., STUIVER, M., VERZINI, S.,
630 LORENZ, D., VAN ROSSUM, M., GOLDFARB, D. & SELENKO, P. 2016. Structural disorder of
631 monomeric alpha-synuclein persists in mammalian cells. *Nature,* 530**,** 45-50,
632 10.1038/nature16531.
633 TREXLER, A. J. & RHOADES, E. 2009. Alpha-synuclein binds large unilamellar vesicles as an
634 extended helix. *Biochemistry,* 48**,** 2304-6, 10.1021/bi900114z.
635 TREXLER, A. J. & RHOADES, E. 2012. N-Terminal acetylation is critical for forming alpha-helical
636 oligomer of alpha-synuclein. *Protein Sci,* 21**,** 601-5, 10.1002/pro.2056.
637 TUTTLE, M. D., COMELLAS, G., NIEUWKOOP, A. J., COVELL, D. J., BERTHOLD, D. A., KLOEPPER, K.
638 D., COURTNEY, J. M., KIM, J. K., BARCLAY, A. M., KENDALL, A., WAN, W., STUBBS, G.,
639 SCHWIETERS, C. D., LEE, V. M., GEORGE, J. M. & RIENSTRA, C. M. 2016. Solid-state NMR

640 structure of a pathogenic fibril of full-length human alpha-synuclein. *Nat Struct Mol Biol,*
641 23**,** 409-15, 10.1038/nsmb.3194.
642 VOLPICELLI-DALEY, L. A., LUK, K. C. & LEE, V. M. 2014. Addition of exogenous alpha-synuclein
643 preformed fibrils to primary neuronal cultures to seed recruitment of endogenous alpha-
644 synuclein to Lewy body and Lewy neurite-like aggregates. *Nat Protoc,* 9**,** 2135-46,
645 10.1038/nprot.2014.143.
646 YAP, T. L., GRUSCHUS, J. M., VELAYATI, A., WESTBROEK, W., GOLDIN, E., MOAVEN, N., SIDRANSKY,
647 E. & LEE, J. C. 2011. Alpha-synuclein interacts with Glucocerebrosidase providing a
648 molecular link between Parkinson and Gaucher diseases. *J Biol Chem,* 286**,** 28080-8,
649 10.1074/jbc.M111.237859.
650